

Coherent Viterbi and Threshold Demodulators for Pulse-Driven GMSK Signals

Kuang Tsai and Gee L. Lui
The Aerospace Corporation
El Segundo, California, USA 90245

Abstract – Pulse-Driven Gaussian Minimum Shift Keying (PDGMSK) was introduced[1] to facilitate a trade between bandwidth efficiency and receiver complexity when using the classical GMSK waveform. The waveform was purposely devised to converge, as data rate decreases, to SDPSK or DPSK without expanding the absolute bandwidth. This paper studies the optimal coherent demodulation of the PDGMSK waveform, and provides simulation results of a near-optimal Viterbi demodulator and a low-complexity threshold demodulator in both single and multiple carrier settings. Trade-off among signal-to-noise ratio (SNR), adjacent channel interference (ACI) level and carrier frequency spacing is also provided.

I. INTRODUCTION

Pulse-Driven Gaussian Minimum Shift Keying (PDGMSK) was originally proposed[1] to accommodate the use of classical GMSK waveform when upgrading an existing military communication system already populated with SDPSK and DPSK receivers. In contrast to the classical GMSK signal, which converges to MSK as data rate decreases, the PDGMSK signal converges to either SDPSK or DPSK depending on whether “Bipolar” or “Unipolar” data pulses are used in generating the waveform. This salient signal feature allows the use of the DPSK-type receivers and provides a backward compatibility with the existing system. The performance of demodulating Unipolar PDGMSK (with $BT=1/2$) using DPSK receiver has been reported in [1] and similar performance can be expected when demodulating Bipolar PDGMSK using SDPSK receiver.

Backward compatibility issue aside, the process of modifying the classic GMSK signal to that of PDGMSK also offers an approach to trade bandwidth efficiency for receiver complexity. For this reason, it is of interest to determine the optimal demodulator for PDGMSK (which in general is not of DPSK-type), and assess its power and bandwidth performance in an FDMA setting. By casting both PDGMSK signals into the well-established framework of Continuous Phase Modulation (CPM) waveforms, this paper details how such signals are optimally demodulated by a Viterbi-algorithm-based trellis demodulator. A simple serial MSK-type threshold demodulator is also considered for purpose of receiver complexity tradeoff. Section 2 reviews the signal definition of PDGMSK and casts it into the CPM waveform framework. Spectral occupancy of PDGMSK is also assessed here via numerical calculation of its theoretical power spectral density (PSD). The near-optimal trellis receiver and the low-complexity threshold receiver are defined in Section 3 in terms of the Laurent Pulse-

Amplitude-Modulation (PAM) signal representation[2]. Section 4 contains bit error rate (BER) simulation data quantifying the performance of the two demodulators.

II. SIGNAL AND SPECTRUM

The Bipolar* PDGMSK waveform is generated by embedding binary NRZ symbols $\{\alpha_n = \pm 1\}$ onto constant-width data pulses of levels $\{\pm 1, 0\}$ – as shown in Figure 1, filtering the resulting pulse stream by a Gaussian filter of bandwidth B , and then frequency-modulating the filter output with modulation index $h=1/2$. A parameter m ($m \geq 1$) is used to designate the data rate of the resulting waveform, which we will simply call PDGMSK- m . Though mathematically unnecessary, the rate designator m is often confined to powers of two (e.g., $m=1, 2, 4$) as the symbol duration of PDGMSK- m is precisely m times that of PDGMSK-1. The symbols $\{\alpha_n\}$ can either be non-coded (i.e., $\alpha_n = d_n$) or pre-coded (i.e., $\alpha_n = (-1)^n d_n d_{n-1}$) where $\{d_n\}$ denotes the source NRZ symbols. Data pre-code does not alter the spectrum of a PDGMSK waveform because equally probable source symbols $\{d_n\}$ always yield equally probable channel symbols $\{\alpha_n\}$ for a binary alphabet with $h=1/2$. However, data pre-code does improve the performance of the demodulators (by averting a performance-degrading differential decoding step at the receiver) and will be assumed throughout this paper.

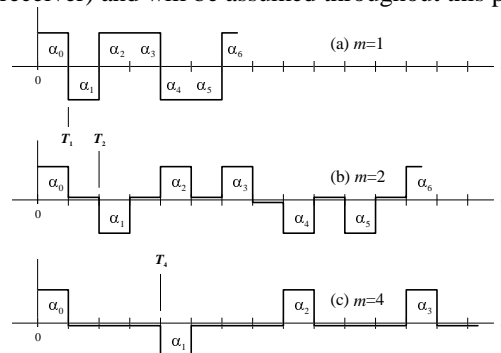


Figure 1. Data Pulses for Generating Bipolar PDGMSK: (a) full-rate, (b) half-rate, (c) quarter-rate.

By definition, PDGMSK-1 is the classical GMSK waveform with symbol duration T_1 set equal to the symbol duration T_c associated with the highest data rate $R_c = 1/T_c$, i.e., $T_1 = T_c$. Also

*This paper only treats the Bipolar PDGMSK waveform explicitly. The Unipolar PDGMSK waveform, which is generated exactly as the Bipolar waveform with a slight change in pulse levels – from $\{\pm 1, 0\}$ to $\{2, 0\}$, can be written as a Bipolar PDGMSK waveform with fixed frequency offset $\Delta f_0 = h/2T_c$ and phase offset $\phi_0 = -\pi h(L-1)/2$. As a result, the signal spectrum and demodulation performance of the Unipolar PDGMSK waveform can readily be inferred from those of Bipolar PDGMSK reported in this paper.

by definition, the symbol duration T_m and symbol rate R_m of PDGMSK- m are related to those of PDGMSK-1 by

$$T_m \equiv m \cdot T_1 = m \cdot T_c \quad (1)$$

$$R_m \equiv 1/T_m = (1/m) \cdot R_1 = (1/m) \cdot R_c \quad (2)$$

It helps to regard PDGMSK-1 as the “parent” waveform from which all “descendant” PDGMSK- m waveforms are derived – each PDGMSK- m ($m>1$) is a lower-rate waveform “devolved” from the highest-rate PDGMSK-1 waveform.

The underlying Gaussian filter is defined in terms of the highest data rate R_c by the (non-causal)[†] impulse response

$$h(t) = \frac{1}{\sqrt{2\pi}\sigma T_c} \cdot \exp\left(-\frac{t^2}{2(\sigma T_c)^2}\right), \quad \sigma \equiv \frac{\sqrt{\ln 2}}{2\pi \cdot B_b} \quad (3)$$

where $B_b \equiv B/R_c = BT_c$ is a dimension-less parameter known as the BT-product, and B is the single-sided 3-dB bandwidth in hertz. As a classic waveform, PDGMSK-1 is completely specified by the well-known GMSK phase pulse

$$q(t) = 1 + \left(\frac{1}{T_c}\right) \cdot \left\{ \begin{array}{l} (t - T_c/2) \cdot \mathcal{Q}\left(\frac{t - T_c/2}{\sigma T_c}\right) - (t + T_c/2) \cdot \mathcal{Q}\left(\frac{t + T_c/2}{\sigma T_c}\right) \\ - \left(\frac{\sigma T_c}{\sqrt{2\pi}}\right) \cdot \left[\exp\left(-\frac{1}{2}\left(\frac{t - T_c/2}{\sigma T_c}\right)^2\right) - \exp\left(-\frac{1}{2}\left(\frac{t + T_c/2}{\sigma T_c}\right)^2\right) \right] \end{array} \right\} \quad (4)$$

$$\mathcal{Q}(x) \equiv \int_x^\infty \left(\frac{1}{\sqrt{2\pi}}\right) \cdot e^{-y^2/2} dy, \quad q(\infty) = 1$$

The time derivative of the GMSK phase pulse, known as the GMSK frequency pulse $f(t)$, is given by

$$f(t) = \left(\frac{1}{T_c}\right) \cdot \left\{ \mathcal{Q}\left(\frac{t - T_c/2}{\sigma T_c}\right) - \mathcal{Q}\left(\frac{t + T_c/2}{\sigma T_c}\right) \right\} \quad (5)$$

where the scaling constant $(1/T_c)$ ensures the normalization condition $q(\infty)=1$. This GMSK frequency pulse is actually the response of the Gaussian filter (3) to a single rectangular pulse $p(t)$ of duration T_c , that is,

$$f(t) = (1/T_c) \cdot [p(t) * h(t)], \quad p(t) = \begin{cases} 1, & |t| < T_c/2 \\ 0, & \text{otherwise.} \end{cases} \quad (6)$$

With P denoting the signal power, h the modulation index and f_c the carrier frequency, the non-devolved PDGMSK-1 waveform being transmitted over the channel is

$$s(t) = \sqrt{2P} \cos[2\pi f_c t + \pi h \cdot \sum_{n \geq 0} \alpha_n q(t - nT_c)] \quad (7)$$

The key to understand the devolved PDGMSK- m waveforms is to note that: (i) the Gaussian filter (3) remains unchanged as the parent waveform devolves, and (ii) the basic rectangular pulse $p(t)$ that gives rise to $f(t)$ – hence $q(t)$ and $s(t)$ – also remains unchanged. [It should be clear from Figure 1 that, as the parent waveform devolves, the only change to the basic rectangular pulse is a longer stretch of trailing zeros which, of course, will not trigger the Gaussian filter to produce non-zero response.] Therefore, accounting for symbol duration expansion, the PDGMSK- m waveform $s_m(t)$ being transmitted over the channel can be formally described by

[†]A time delay in the amount of $(L/2)T_c$, where $L \equiv \lceil 1/B_b \rceil$, will render the Gaussian filter essentially causal. We adhere to the non-causal formulation throughout this paper for the sake of simpler notations. The B_b -dependent time delay can always be applied when needed.

$$s_m(t) = \sqrt{2P} \cos[2\pi f_c t + \pi h \cdot \sum_{n \geq 0} \alpha_n q_m(t - nT_m)] \quad (8)$$

where $q_m(t)$ denotes the phase pulse of PDGMSK- m . However, since the only difference between waveforms (8) and (7) lies in the symbol duration $T_m = mT_c$, and since the underlying phase pulse $q(t)$ defined in (4) is common to all PDGMSK- m waveforms (i.e., $q_m(t) = q(t)$ in absolute time scale), an equivalent expression of (8) is

$$s_m(t) = \sqrt{2P} \cos[2\pi f_c t + \pi h \cdot \sum_{n \geq 0} \alpha_n q(t - nT_m)] \quad (9)$$

Normalized Phase Pulse of PDGMSK

Since the symbol duration T_m varies with m , and since data demodulation is intrinsically a per-symbol operation, it is more pertinent to express the common phase pulse $q_m(t) = q(t)$ in a “ T_m -normalized” time scale. To this end we define an m -specific normalized time $\tau = (t/T_m)$, and use (4) and (1) to arrive at a normalized phase pulse $\underline{q}_m(\tau)$ for each of the PDGMSK- m ($m \geq 1$) waveforms:

$$\underline{q}_m(\tau) \equiv q(\tau \cdot T_m) = 1 + \left\{ \begin{array}{l} (m\tau - 1/2) \cdot \mathcal{Q}\left(\frac{m\tau - 1/2}{\sigma}\right) - (m\tau + 1/2) \cdot \mathcal{Q}\left(\frac{m\tau + 1/2}{\sigma}\right) \\ - \left(\frac{\sigma}{\sqrt{2\pi}}\right) \cdot \left[\exp\left(-\frac{1}{2}\left(\frac{m\tau - 1/2}{\sigma}\right)^2\right) - \exp\left(-\frac{1}{2}\left(\frac{m\tau + 1/2}{\sigma}\right)^2\right) \right] \end{array} \right\} \quad (10)$$

Note that $\underline{q}_1(\tau)$ is exactly the T_c -normalized version of (4):

$$\underline{q}_1(\tau) \equiv q(\tau \cdot T_c) = 1 + \left\{ \begin{array}{l} (\tau - 1/2) \cdot \mathcal{Q}\left(\frac{\tau - 1/2}{\sigma}\right) - (\tau + 1/2) \cdot \mathcal{Q}\left(\frac{\tau + 1/2}{\sigma}\right) \\ - \left(\frac{\sigma}{\sqrt{2\pi}}\right) \cdot \left[\exp\left(-\frac{1}{2}\left(\frac{\tau - 1/2}{\sigma}\right)^2\right) - \exp\left(-\frac{1}{2}\left(\frac{\tau + 1/2}{\sigma}\right)^2\right) \right] \end{array} \right\} \quad (11)$$

From (10) and (11) we arrive at

$$\underline{q}_m(\tau) = \underline{q}(m\tau) \quad (12)$$

which concisely describes how the PDGMSK- m waveform converges to SDPSK: as m increases, $\underline{q}_m(\tau)$ converges to an unit step function, thus inducing an abrupt phase change of $\pm\pi h = \pm\pi/2$ at the symbol boundaries as in SDPSK. Figure 2 depicts a few normalized phase pulses using $B_b = 1/6 \equiv 1/L$.

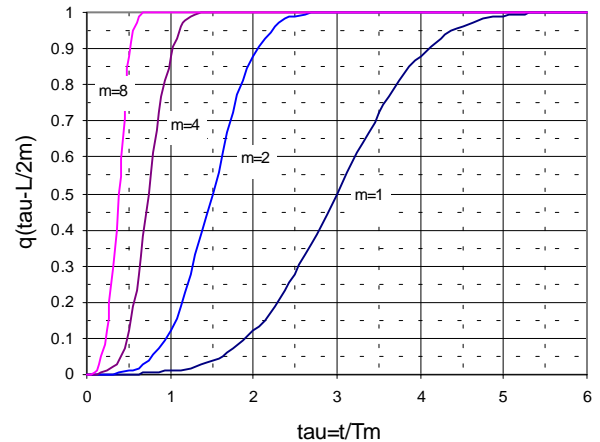


Figure 2. Normalized Phase Pulses of PDGMSK.

[An time delay of $(L/2m)T_m$ has been injected in each of the normalized phase pulses to ensure system causality, i.e., Figure 2 are plots for $\underline{q}_m(\tau - (L/2m)) = q(t - (L/2)T_c)$.]

Power Spectral Density of PDGMSK

Given the normalized phase pulse $q_m(\tau)$, it is straightforward to compute the PSD for the PDGMSK- m waveform. In fact, in view of (12), the same closed-form formula used in [3] for computing the theoretical PSD of general CPM waveforms is directly applicable provided the governing CPM phase pulse is replaced by $q_m(\tau)$. Figure 3 depicts a few PSDs obtained in this manner; the PSD of SDPSK (shown in +'s) is also included for comparison.

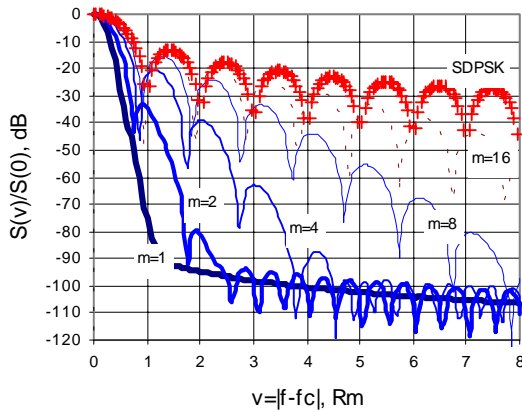


Figure 3. R_m -Normalized PSD for PDGMSK.

The frequency-axis in Figure 3 is normalized with respect to the symbol rate R_m to facilitate a fair spectral comparison between the PDGMSK- m and SDPSK waveforms. Figure 3 shows that, when signaling at the same rate R_m , the PDGMSK- m waveform is spectrally more efficient than the SDPSK waveform. On the other hand, for absolute bandwidth consideration, the PSDs in Figure 3 should be plotted against a frequency-axis normalized with respect to R_c , instead of R_m . This is depicted in Figure 4 where the absolute spectral occupancy of every descendant PDGMSK- m waveform is seen to be strictly upper-bounded by that of its parent GMSK waveform.

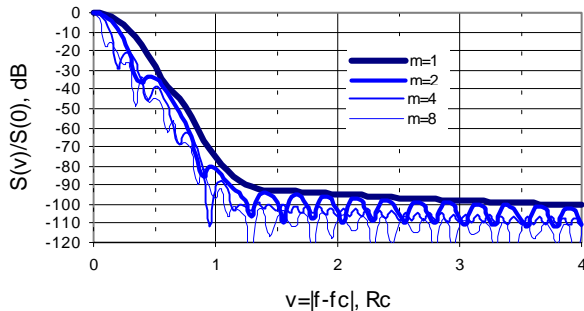


Figure 4. R_c -Normalized PSD for PDGMSK.

III. VITERBI AND THRESHOLD DEMODULATORS

The basis of demodulating PDGMSK using PAM-based coherent Viterbi receiver is the fact that every PDGMSK- m waveform is actually a CPM waveform. In view of (12), the

PAM-based trellis[4,7] and threshold[5,8] demodulators used for receiving the classic GMSK waveform is clearly applicable provided the underlying GMSK phase pulse is replaced by $q_m(\tau)$. This phase pulse replacement changes the generalized phase pulse[6] $c(\tau) \equiv c^{(1)}(\tau)$ of the classic GMSK waveform into that of the PDGMSK- m waveform[‡]:

$$c^{(m)}(\tau) \equiv \begin{cases} \sin[\pi h - \pi h q_m(|\tau - L/2m|)] / \sin(\pi h); & |\tau| \leq L/m \\ 0 & |\tau| \geq L/m \end{cases} \quad (13)$$

which, in turn, changes all the Laurent PAM-filters such as

$$h_0^{(m)}(\tau) = \prod_{i=1}^L c^{(m)}(\tau - i/m) \quad (14)$$

$$h_1^{(m)}(\tau) = h_0^{(m)}(\tau) \cdot \frac{c^{(m)}(\tau + 1/m)}{c^{(m)}(\tau - (L-1)/m)} \quad (15)$$

Figure 5 depicts a few PDGMSK generalized phase pulses (13) using $B_v=1/6 \equiv 1/L$, and Figure 6 depicts the corresponding PAM-filters (14) and (15) along with their respective energy levels. The vertical axis on the right edge of Figure 6 is intended for the second PAM-filter (15), shown in dash, which generally carries much low energy than (14). [Filter $h_1^{(2)}(\tau)$ barely registers in this magnified scale, and filter $h_1^{(4)}(\tau)$ is not even visible in Figure 6!] These low filter energy levels suggest that a threshold receiver (which is equivalent to a one-filter trellis receiver) can perform nearly as well as a two-filter trellis receiver when demodulating the PDGMSK- m waveforms with $m \geq 2$. [This, in fact, is confirmed by simulation results presented later.]

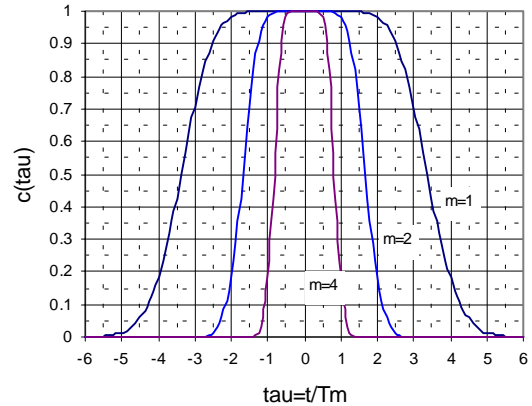


Figure 5. Generalized Phase Pulse for PDGMSK.

[‡]Equations (13)–(15) are given in terms of the normalized time $\tau=t/T_m$ – setting $m=1$ yields corresponding equations for classic GMSK. The $(L/2m)$ “shift factor” used in (13) is exactly the causality-forging time delay injected earlier when plotting the normalized phase pulses (10) in Figure 2. The time support of (13) is $[-L/m, +L/m]$, and those for the PAM-filters (14) and (15) are $[0, (L+1)/m]$ and $[0, (L-1)/m]$, respectively.

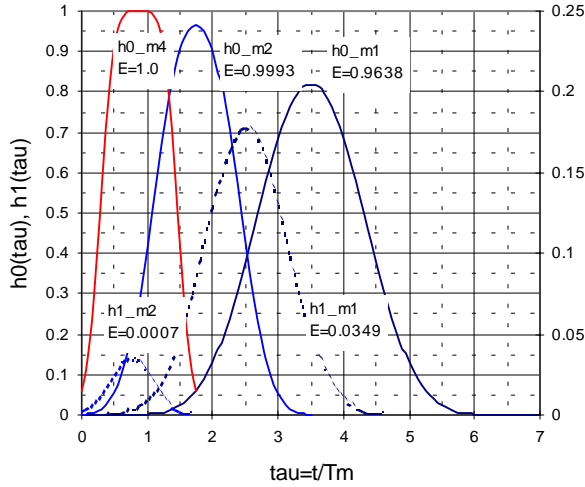


Figure 6. PAM Filters for PDGMSK.

With pre-coded channel symbols $\alpha_n = (-1)^n \cdot d_n d_{n-1}$, the branch metric for the PAM-based 2-filter trellis demodulator is given by

$$\lambda(n) = \lambda(v_n, v_{n-1}) = \begin{cases} \text{Im}(r_{0,n}) \cdot d_n - \text{Re}(r_{1,n}) \cdot d_n d_{n-1} d_{n-2} & n: \text{even} \\ \text{Re}(r_{0,n}) \cdot d_n - \text{Im}(r_{1,n}) \cdot d_n d_{n-1} d_{n-2} & n: \text{odd} \end{cases} \quad (16)$$

where $v_n = (d_n, d_{n-1})$ denotes the state of the underlying Viterbi algorithm, $r_{k,n}$ ($k=0,1$) denotes the (complex) output of the PAM-filters (14) and (15) at time $t=nT_m$:

$$r_{k,n} \equiv \int_{-\infty}^{\infty} z_r(t) \cdot h_k^{(m)}(t - nT_m) dt, \quad (17)$$

and $z_r(t)$ denotes the complex envelope of the transmit signal (8) corrupted by additive white Gaussian noise (AWGN). The Viterbi algorithm functions as a maximum likelihood sequence estimator, and recursively produces sub-optimal[§] state sequence $\{v_n\}$ conveying the demodulated symbol \underline{d}_n . The 1-filter trellis demodulator, defined by (16) with all $r_{1,n}$ -related terms suppressed, is readily seen to be equivalent to the following simple threshold demodulator:

$$\underline{d}_n = \begin{cases} +1, & \rho_n \geq 0 \\ -1, & \rho_n < 0 \end{cases} \quad (18)$$

where ρ_n denotes the alternating-inphase-quadrature (AIQ) output of the principal Laurent PAM-filter at time $t=nT_m$:

$$\rho_n = \begin{cases} \text{Im}(r_{0,n}) & n: \text{even} \\ \text{Re}(r_{0,n}) & n: \text{odd} \end{cases} \quad (19)$$

The threshold demodulator is a practical low-complexity alternative to the 2-filter trellis demodulator: the associated performance degradation is either negligible (for large BT-products such as $B_b \geq 1/3$) or can be made small via least-mean-square equalization[7].

[§]A total of $Q=2^{L-1}$ PAM-filters, and a matching 2^L -state Viterbi algorithm, are needed in order to achieve true-optimal demodulation performance. The 2-filter trellis demodulator, shown near-optimal through extensive simulations, represents a reasonable trade-off between demodulation performance and receiver complexity.

IV. SIMULATION RESULTS

Simulation programs based on a 2-filter trellis demodulator (TRLS_F2) and a 1-filter threshold demodulator (AIQ_F1) are developed to assess the BER performance of the PDGMSK- m waveforms in AWGN, both with and without ACI. Only simulation data for the cases of $m=1, 2$ (with a parent waveform of $B_b=1/6$) are presented for illustration. All results are based upon 16 samples per symbol simulation runs, with each BER estimate recorded upon reaching 1000 symbol error counts. Data pre-code $\alpha_n = (-1)^n \cdot d_n d_{n-1}$ is assumed in all simulations.

AWGN Performance

Figure 7 depicts the AWGN performance of PDGMSK- m when using TRLS_F2 and AIQ_F1. Note that while TRLS_F2 significantly outperforms AIQ_F1 in the case of $m=1$ (e.g., 3.2 dB at BER=0.01), the threshold-based AIQ_F1 performs equally well as the trellis-based TRLS_F2 when $m=2$. This, as alluded earlier by the low energy level of the second PAM-filter, is not at all surprising, and the same can be expected for PDGMSK- m with larger m . Also note that, in the case of $m=2$, the threshold-based AIQ_F1 already performs nearly as well as ideal BPSK. This implies that, when it comes to demodulating PDGMSK- m with $m \geq 2$ and $B_b \geq 1/6$, there is no practical need to enhance the performance of the low-complexity AIQ_F1 via least-mean-square equalization – except possibly when the required BER is much lower than 0.001.

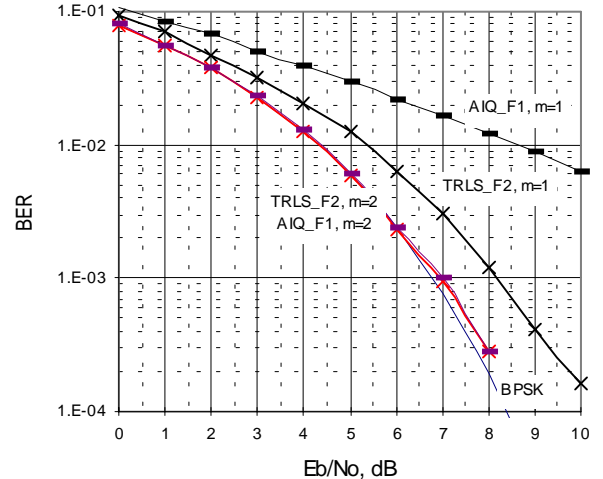


Figure 7. AWGN Performance of PDGMSK.

ACI Performance

To assess the ACI performance of PDGMSK waveform we consider a typical FDMA interference scenario in which a desired PDGMSK- m signal is “surrounded” by two identically modulated PDGMSK- m signals. Both interfering signals are equally separated from the desired signal in frequency (one on each side) with an A_i dB power advantage over the desired signal. $[A_i]$ can be used to account for the possible difference in propagation loss between the desired

and the interfering signals. It can also be used to model the worst-case power fluctuation between the signals.] Figure 8 depicts the SNR required to attain a 0.01 operating BER in terms of the underlying carrier spacing d_f (in units of R_m) for both $A_I=0$ and $A_I=25$ dB. The desired PDGMSK- m signal is demodulated using TRLS_F2 and AIQ_F1 for $m=1$ and $m=2$, respectively.

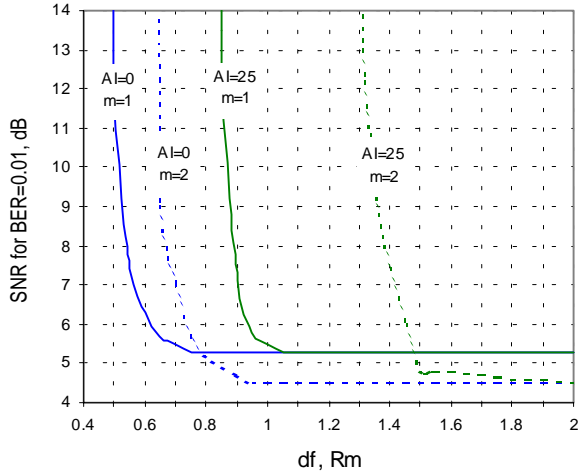


Figure 8. ACI Performance, R_m -Normalized.

An intuitive power-versus-bandwidth tradeoff is evident in each of these curves: as multiple signals are packed closer to achieve higher throughput, more signal power must be expended in order to maintain a given BER; and a minimum packing separation exists below which no amount of power increase is enough to attain the desired BER. Figure 8 indicates that, for a fixed A_I , the descendant PDGMSK-2 waveform is spectrally less efficient than its parent GMSK waveform on a R_m -normalized basis. This is not surprising in view of Figure 3. A R_c -normalized version of Figure 8 is given in Figure 9 for absolute bandwidth consideration.

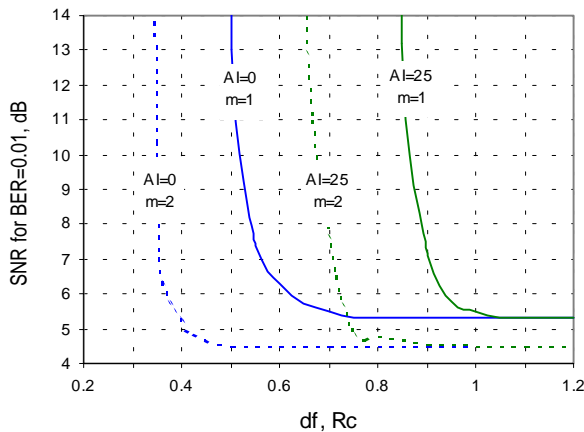


Figure 9. ACI Performance, R_c -Normalized.

V. CONCLUSIONS

Optimal coherent demodulation of the PDGMSK waveform has been determined in this paper. We have quantified the spectral occupancy of the signal, and demonstrated how such signal can be efficiently demodulated using a near-optimal trellis receiver and a low-complexity threshold receiver. While the absolute spectral occupancy of any descendant PDGMSK waveform is narrower than that of its parent GMSK waveform, every PDGMSK waveform is spectrally more compact than the SDPSK waveform signaling at the same data rate. We have quantified the BER performance of these receivers in AWGN, both with and without ACI. We have also shown that every descendant PDGMSK waveform devolved from a parent GMSK waveform with a BT-product $B_T \geq 1/6$ can be demodulated using the low-complexity threshold receiver with near-BPSK performance.

REFERENCES

- [1] R. Rhodes, K. Hetling, "Pulse Driven Gaussian Minimum Shift Keying," *Proceedings MILCOM98*, pp. 511-514, October 1998.
- [2] P. Laurent, "Exact Approximation Construction of Digital Phase Modulations by Superposition of Amplitude Modulated Pulses (AMP)," *IEEE Transactions on Communications*, Vol. 34, No. 2, February, 1986.
- [3] J. Anderson, T. Aulin and C. Sundberg, *Digital Phase Modulation*, Plenum, New York, 1986.
- [4] K. Tsai and G. L. Lui, "Coherent Demodulation Performance of 2-ary and 4-ary GMSK Using Viterbi Algorithm-based Receivers," *Classified Proceedings MILCOM98*, October 1998.
- [5] G. L. Lui, "Threshold Detection Performance of GMSK Signal with $BT=0.5$," *Proceedings MILCOM98*, pp. 515-519, October 1998.
- [6] U. Megali and M. Morelli, "Decomposition of M-ary CPM Signals into PAM Waveforms," *IEEE Transactions on Communications*, Vol. 41, No. 5, September, 1995.
- [7] K. Tsai and G. L. Lui, "Binary GMSK - Characteristics and Performance," *Proceedings ITC'99*, October 1999.
- [8] G. L. Lui and K. Tsai, "Viterbi and Serial Demodulators for Pre-coded Binary GMSK," *Proceedings ITC'99*, October 1999.